

# DBGSL: Dynamic Brain Graph Structure Learning

Alexander Campbell<sup>1,2</sup>, Antonio Giuliano Zippo<sup>5</sup>, Luca Passamonti<sup>1</sup>, Nicola Toschi<sup>3,4</sup>, Pietro Liò<sup>1</sup>

<sup>1</sup>University of Cambridge, <sup>2</sup>The Alan Turing Institute <sup>3</sup>University of Rome Tor Vergata, <sup>4</sup>A.A. Martinos Center for Biomedical Imaging, Harvard Medical School <sup>5</sup>Institute of Molecular Bioimaging and Physiology, National Research Council

## Abstract

Functional connectivity (FC) between regions of the brain is commonly estimated through statistical dependency measures applied to functional magnetic resonance imaging (fMRI) data. The resulting functional connectivity matrix (FCM) is often taken to represent the adjacency matrix of a brain graph. Recently, graph neural networks (GNNs) have been successfully applied to FCMs to learn brain graph representations. A common limitation of existing GNN approaches, however, is that they require the graph adjacency matrix to be known prior to model training. As such, it is implicitly assumed the ground-truth dependency structure of the data is known. Unfortunately, for fMRI this is not the case as the choice of which statistical measure best represents the dependency structure of the data is non-trivial. Also, most GNN applications to fMRI assume FC is static over time, which is at odds with neuroscientific evidence that functional brain networks are time-varying and dynamic. These compounded issues can have a detrimental effect on the capacity of GNNs to learn representations of brain graphs. As a solution, we propose Dynamic Brain Graph Structure Learning (DBGSL), a supervised method for learning the optimal time-varying dependency structure of fMRI data. Specifically, DBGSL learns a dynamic graph from fMRI timeseries via spatial-temporal attention applied to brain region embeddings. The resulting graph is then fed to a spatial-temporal GNN to learn a graph representation for classification. Experiments on large resting-state as well as task fMRI datasets for the task of gender classification demonstrate that DBGSL achieves state-of-the-art results outperforming the best baseline in terms of accuracy by 5.16 and 8.38 percentage points, respectively. Moreover, analysis of the learnt dynamic graphs highlights prediction-related brain regions which align with findings from existing neuroscience literature. Overall, our findings highlight the benefit of learning a dynamic dependency structure for GNN-based models of fMRI data.

## Introduction

Functional magnetic resonance imaging (fMRI) is primarily used to measure blood-oxygen level dependent (BOLD) signal (or blood flow) in the brain. It is one of the most commonly used non-invasive imaging techniques to investigate brain function. Typically, this is accomplished by using a statistical measure of pairwise dependence (e.g. Pearson correlation, partial correlation, mutual information) to measure the functional connectivity (FC) between BOLD time-

series of anatomically separated regions of the brain over time (Friston 1994; Wang et al. 2016). The resulting functional connectivity matrices (FCMs), (or functional connectomes) are commonly used either in graph-based network analyses (Sporns 2022; Wang, Zuo, and He 2010) or more recently as inputs to machine learning algorithms (Yan et al. 2020; He et al. 2020) in order to provide insights into brain function and dysfunction.

Graph neural networks (GNNs) are a type of deep neural network capable of learning representations of graph-structured data (Wu et al. 2020a). Following a message-passing scheme, GNNs aggregate information from neighbors on an observed graph structure - represented by an adjacency matrix - in order to learn a graph representation. Recently, GNNs have been used to learn representations of the brain by pre-processing FCMs into adjacency matrices corresponding to brain graphs (Azevedo et al. 2022; Kim, Ye, and Kim 2021). These representations have been successfully used to predict subject phenotypes such as gender (Kim and Ye 2020) and age (Gadgil et al. 2020), when the brain is performing different cognitive tasks (Zhang et al. 2021), and brain disorders such as autism spectrum disorder (ASD) (Li et al. 2021) and attention deficit hyperactivity disorder (ADHD) (Zhao et al. 2022).

Despite the growing application of GNNs to fMRI data, a major limitation is the requirement that the graph adjacency matrix is known prior to model training. It is therefore implicitly assumed that FCMs represent the ground-truth dependency structure of fMRI data. In reality, however, this is not the case, as FCMs are highly dependent on the choice of measure used to quantify statistical dependence (Wang et al. 2014) as well as on any pre-processing steps, such as thresholding or binarization, which are commonly used to simplify the matrix (Korhonen, Zanin, and Papo 2021). As such, brain regions may appear functionally connected under one combination of pre-processing steps but disconnected under another (Mohanty et al. 2020). Moreover, to date the majority of GNN works use FCMs that capture only static FC (Zhang et al. 2021; Kim, Ye, and Kim 2021), despite growing neuroscientific evidence that FC dynamically changes over time (Chang and Glover 2010; Calhoun et al. 2014). This suggests important potential benefits in choosing a measure of dynamic FC (Mohanty et al. 2020) in order to create time-varying dynamic adjacency matrices

for GNN-based models applied to fMRI data. Thus, to ensure GNNs are able to learn useful representations of brain graphs, it is of high priority to establish the most appropriate way to construct prior FCMs from fMRI data.

A promising solution to the problem of defining the correct prior dependency structure of a dataset for GNNs is deep graph structure learning (GSL) (Zhu et al. 2021). GSL is a framework that learns the adjacency matrix of a dataset alongside the parameters of a GNN by solving a downstream task such as classification or regression. Several recent attempts at applying GSL methods to timeseries data have shown improved performance on regression tasks (Cao et al. 2020; Wu et al. 2020b, 2019). However, the dependency structure of the data is still assumed to be static over time. To this end, we propose **Dynamic Brain Graph Structure Learning (DBGSL)**, an end-to-end trainable model that can learn task-specific dynamic brain graphs from region-wise BOLD timeseries derived from fMRI data in a supervised framework.

We summarize the contributions of this paper as follows:

- To the best of our knowledge, DBGSL is the first end-to-end trainable GNN-based model to learn a dynamic graph representing the dependency structure of multivariate timeseries data.
- Specifically, DBGSL constructs dynamic graph adjacency matrices using spatial-temporal attention applied to brain region embeddings learnt from fMRI data.
- In addition, DBGSL learns the optimal amount of edge sparsity for constructing adjacency matrices thereby avoiding arbitrary thresholding post-training and maximizing efficiency and interpretability.
- Moreover, for the task of gender classification on resting-state and task fMRI datasets, DBGSL achieves state-of-the-art performance outperforming the best baseline in terms of accuracy by 5.16 and 8.38 percentage points (pp), respectively.
- Finally, an interpretability analysis of the dynamic adjacency matrices learnt by DBGSL reveals gender-discriminative brain regions that align with findings from existing neuroscience literature.

## Related work

Our proposed model, DBGSL, builds upon related work from the field of GSL as well as deep learning methods for fMRI data, particularly those using recurrent neural networks (RNNs), convolutional neural networks (CNNs), and graph neural networks (GNNs).

**Recurrent & convolutional neural networks** Since region-wise BOLD signals derived from fMRI data are a multivariate timeseries, RNN variants that use long-short term memory (LSTM) (Hochreiter and Schmidhuber 1997) or gated recurrent unit (GRU) (Cho et al. 2014) have been widely used on fMRI data (Hebling Vieira et al. 2021; Gao and No 2022). However, the ability of RNNs to learn complex temporal dependencies comes at the cost of neglecting to explicitly learn region-wise spatial dependencies. To learn directly from FCMs, Kawahara et al. (2017) propose novel

CNN kernels that can exploit localised topology. However, recent benchmark studies show that these kernels can be easily outperformed by simple linear models (He et al. 2020). To date, only Fan et al. (2020) have applied RNNs combined with CNNs to learn from dynamic FCMs. However, the quadratic increase in the number of parameters from taking vectorized FCMs (i.e. lower triangle) as input to CNNs makes such an approach computationally infeasible for a large number of brain regions. Recently, temporal convolutional networks (TCNs) (Oord et al. 2016), utilizing one-dimensional (1D) convolutional kernels, have shown improved performance over RNNs when used for feature extraction on BOLD timeseries for downstream classification tasks (Azevedo et al. 2022).

**Graph neural networks** The majority of GNN-based methods for learning representations of brain graphs use static FCMs estimated using either Pearson correlation (Zhang et al. 2021; Kim and Ye 2020; Azevedo et al. 2022; Huang et al. 2022) or partial correlation (Li et al. 2021). Not only does this ignore the evidence that FC is dynamic and changes over time (Calhoun et al. 2014), but also classification performance is tied to the choice of FC measure, a non-trivial task (Korhonen, Zanin, and Papo 2021). More recently, methods for specifically learning representations of dynamic brain graphs have emerged in an attempt to model the non-stationary nature of FC. In particular, Gadgil et al. (2020) propose a spatial-temporal graph convolutional network which interleaves GNN layers with CNN layers. However, only graph node features are taken to be time-varying whilst the adjacency matrix is assumed to be static. On the other hand, Kim, Ye, and Kim (2021) propose a transformer-inspired network with specially designed spatial and temporal attention mechanisms for dynamic brain graphs. Still, the employed measure of dynamic FC is Pearson correlation and the model requires the graph adjacency matrices to be unweighted (i.e. binarized).

**Graph structure learning** Several methods using deep learning for GSL have been proposed (Zhu et al. 2021). Specifically, for supervised tasks on timeseries data, the adjacency matrix is either sampled from a probabilistic model with learnable parameters (Shang, Chen, and Bi 2021; Franceschi et al. 2019), constructed from a learnable lower dimensional embedding (Wu et al. 2020b), or fully parameterized and iteratively updated from an initial estimate (Wu et al. 2019). Unlike DBGSL, these previous approaches do not learn to infer the dependency structure directly from timeseries data. As such, the learnt adjacency matrix is global, meaning it cannot be interpreted at an instance or per sample basis in order to examine class differences which are, for instance, useful for discovering disease biomarkers. Although some recent attempts have been made at learning brain graphs from BOLD timeseries derived for fMRI data (Mahmood et al. 2021; Riaz et al. 2020; Kan et al. 2022; Zhang and Huang 2019; Jie et al. 2020), the graph adjacency matrix is assumed to be static over time.

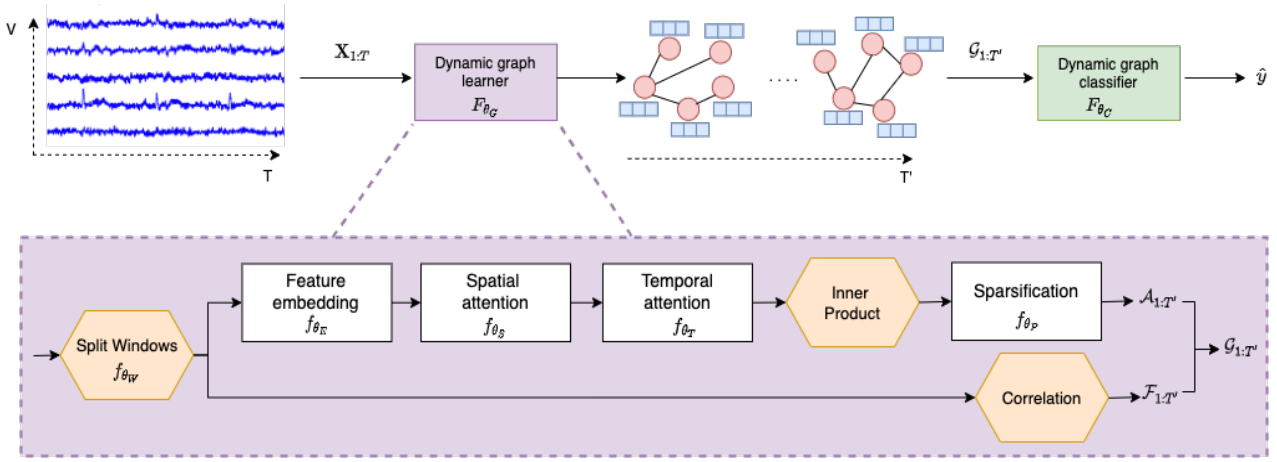


Figure 1: The conceptual framework of DBGSL.

## Problem formulation

We formulate dynamic GSL in terms of a supervised multivariate timeseries classification problem. Let  $\mathbf{X}_{1:T} = (\mathbf{x}_1 \dots \mathbf{x}_T) \in \mathbb{R}^{V \times T}$  denote a multivariate timeseries of BOLD signals from  $V$  regions of the brain over  $T$  timepoints and  $y \in [0, \dots, C-1]$  a corresponding class label. Suppose there exists an unknown dependency structure between brain regions that evolves over time. We assume the dependency structure can be described by a dynamic brain graph  $G_{1:T'} = (\mathcal{A}_{1:T'}, \mathcal{F}_{1:T'})$  consisting of a dynamic adjacency matrix  $\mathcal{A}_{1:T'} = (\mathbf{A}_1, \dots, \mathbf{A}_{T'})$  and dynamic node features  $\mathcal{F}_{1:T'} = (\mathbf{F}_1, \dots, \mathbf{F}_{T'})$ . Each adjacency matrix  $\mathbf{A}_t \in \mathbb{R}_{\geq 0}^{V \times V}$  defines the pairwise connection strength between brain regions and the feature matrix  $\mathbf{F}_t \in \mathbb{R}^{V \times B}$  ascribes each brain region  $B$  features. We let  $T' \leq T$  to accommodate the fact that brain regions tend to change at a lower repetition time (TR) i.e., the time between the acquisition of one fMRI volume to the next. Given a dataset  $\mathcal{D}$  of  $|\mathcal{D}| = N$  subjects fMRI data, our aim is to train a model  $F_{\theta}(\cdot) = F_{\theta_G} \circ F_{\theta_C}(\cdot)$  with parameters  $\theta = \theta_G \cup \theta_C$  that maps BOLD timeseries to a dynamic brain graph  $F_{\theta_G}(\mathbf{X}_{1:T}) = G_{1:T'}$  which can be used to predict a class label  $F_{\theta_C}(G_{1:T'}) = \hat{y}$  for each subject. Training consists of minimizing the discrepancy between the actual label  $y$  and the predicted label  $\hat{y}$ , described by a loss function  $\mathcal{L}(y, \hat{y})$ . The optimization objective is  $\theta^* = \arg \min_{\theta} \mathbb{E}_{(\mathbf{X}_{1:T}, y) \in \mathcal{D}} [\mathcal{L}(y, F_{\theta}(\mathbf{X}_{1:T}))]$ .

## Method

As shown in Figure 1, DBGSL consists of two components: (1) dynamic graph learner  $F_{\theta_G}(\cdot)$ , and (2) dynamic graph classifier  $F_{\theta_C}(\cdot)$ . We henceforth expand upon the architecture of each component and set-out the training objective.

### Dynamic graph learner

**Split windows** The BOLD timeseries  $\mathbf{X}_{1:T}$  are first split into windows using a window function  $f_{\theta_w}(\cdot)$  with hyperparameters  $P$  and  $S$  denoting window length and stride, re-

spectively. More formally,

$$f_{\theta_w}(\mathbf{X}_{1:T}) = \tilde{\mathcal{X}}_{1:T'} = (\tilde{\mathbf{X}}_1, \dots, \tilde{\mathbf{X}}_{T'}) \quad (1)$$

$$\tilde{\mathbf{X}}_t = \mathbf{X}_{tS:tS+P}, \quad t = 1, \dots, T'$$

where  $\tilde{\mathcal{X}}_{1:T'} \in \mathbb{R}^{P \times V \times T'}$  represents a stacked timeseries of windows of length  $P$  over timepoints  $T' = \lfloor (T - 2(P-1) - 1) / S + 1 \rfloor$ . As a rule of thumb, the window length is typically set between 100 and 40 seconds and stride between 1 and 5 seconds (Zalesky and Breakspear 2015) to avoid mapping spurious connectivity fluctuations.

**Brain region embeddings** The windowed timeseries is next transformed into a  $K_E$ -dimensional brain region embedding  $f_{\theta_E}(\tilde{\mathcal{X}}_{1:T'}) = \tilde{\mathcal{E}}_{1:T'}$  where  $\tilde{\mathcal{E}}_{1:T'} = (\tilde{\mathbf{E}}_1, \dots, \tilde{\mathbf{E}}_{T'}) \in \mathbb{R}^{K_E \times V \times T'}$ . To achieve this, first each window  $\tilde{\mathbf{X}}_t$  is transformed into a  $K_G$ -dimensional embedding  $\mathbf{H}_t^{(1)} \in \mathbb{R}^{K_G \times V}$  using a linear layer

$$\mathbf{H}_t^{(1)} = \mathbf{W}_1^E \tilde{\mathbf{X}}_t + \mathbf{b}_1^E \quad (2)$$

where  $\mathbf{W}_1^E \in \mathbb{R}^{K_G \times P}$  and  $\mathbf{b}_1^E \in \mathbb{R}^{K_G}$  are trainable weight and bias parameters which are shared across brain regions and timepoints. Next, to ensure each embedding includes temporal information at the window frequency,  $\mathcal{H}_{1:T'}^{(1)} = (\mathbf{H}_1^{(1)}, \dots, \mathbf{H}_{T'}^{(1)}) \in \mathbb{R}^{K_G \times V \times T'}$  is input to an inception TCN (I-TCN) adapted from Wu et al. (2020b). Specifically, an I-TCN takes the 1D dilated convolutional kernels and causal padding from TCN (Oord et al. 2016) and combines it with an inception structure (Szegedy et al. 2015). More formally, suppose I-TCN consists of  $L_G$  layers, then for the  $l$ -th layer with  $M$  convolutional filters we have

$$\mathcal{H}_{1:T'}^{(l+1)} = \text{ReLU}(\text{BatchNorm}(\|_{m=1}^M \mathcal{H}_{1:T'}^{(l)} *_d \mathcal{F}_m^{(l)})) \quad (3)$$

where  $\mathcal{H}_{1:T'}^{(l)}, \mathcal{H}_{1:T'}^{(l+1)} \in \mathbb{R}^{K_G \times V \times T'}$  are input and output brain region embeddings,  $\mathcal{F}_m^{(l)} \in \mathbb{R}^{\lfloor K/M \rfloor \times K \times S_m}$  is the  $m$ -th 1D convolutional filter of length  $S_m$ ,  $\|$  denotes concatenation along the feature dimension,  $*_d$  denotes convolution along the time dimension with dilation factor  $d$ , and

BatchNorm( $\cdot$ ), ReLU( $\cdot$ ) denote batch normalization (Ioffe and Szegedy 2015) and the rectified linear activation function (Hahnloser et al. 2000), respectively. We set  $d = 2^{l-1}$  which increases the receptive field size of each convolutional kernel exponentially with the number of layers  $L_G$  and enforce  $S_1 < S_2 < \dots < S_M$  to allow for the simultaneous use of small kernel sizes to learn short-term temporal patterns and larger kernels to learn long-term patterns within a single layer. The final embedding  $\tilde{\mathcal{E}}_{1:T'}$  is obtained following two more linear layers

$$\bar{\mathbf{E}}_t = \mathbf{W}_3^E (\text{ReLU}(\mathbf{W}_2^E \mathbf{H}_t^{(L_G)} + \mathbf{b}_2^E) + \mathbf{b}_3^E) \quad (4)$$

where  $\mathbf{W}_2^E \in \mathbb{R}^{K_G \times K_G}$ ,  $\mathbf{b}_2^E \in \mathbb{R}^{K_G}$ , and  $\mathbf{W}_3^E \in \mathbb{R}^{K_E \times K_G}$ ,  $\mathbf{b}_3^E \in \mathbb{R}^{K_E}$ .

**Spatial attention** Since the I-TCN extracts features from each brain region BOLD timeseries independently, we account for inter regional or spatial relationships using a novel spatial attention mechanism  $f_{\theta_S}(\cdot)$  adapted from squeeze-and-excite attention networks (Hu, Shen, and Sun 2018). Given the temporal slicing of brain region embeddings  $\tilde{\mathcal{E}}_{1:T'} = (\bar{\mathbf{E}}_1, \dots, \bar{\mathbf{E}}_{T'})$ , we define a spatial attention score vector

$$\mathbf{u}_t = \text{Sigmoid}(\text{ReLU}(\phi \bar{\mathbf{E}}_t \mathbf{W}_1^S) \mathbf{W}_2^S) \quad (5)$$

where Sigmoid( $\cdot$ ) denotes sigmoid activation function,  $\phi^\top = [1/K_E, \dots, 1/K_E]$  takes an average over  $K_E$  features for each brain region  $\phi \bar{\mathbf{H}}_t \in \mathbb{R}^V$ , and the trainable weight parameters  $\mathbf{W}_1^S \in \mathbb{R}^{V \times \tau V}$  and  $\mathbf{W}_2^S \in \mathbb{R}^{\tau V \times V}$  encode brain region dependencies via a bottleneck controlled by the hyperparameter  $\tau \in (0, 1]$ . The resulting spatial attention score vector  $\mathbf{u}_t \in [0, 1]^V$  is reshaped and used to reweight the original brain region feature embeddings following

$$\hat{\mathcal{E}}_{1:T'} = [\bar{\mathbf{E}}_1 \odot \mathbf{U}_1, \dots, \bar{\mathbf{E}}_{T'} \odot \mathbf{U}_{T'}] \quad (6)$$

where  $\mathbf{U}_t \in \mathbb{R}^{1 \times V}$  and  $\odot$  denotes elementwise multiplication. Clearly each element of  $\mathbf{u}_t$  describes the importance of a brain region at a given timepoint.

**Temporal attention** Furthermore, to emphasise timepoints with the most important brain region embeddings we employ a temporal attention mechanism  $f_{\theta_T}(\cdot)$ . The spatially attended brain region features are first reshaped into a matrix  $\hat{\mathbf{E}}_{1:T'} \in \mathbb{R}^{K_E V \times T'}$  and then a temporal attention score vector and subsequent reweighting are computed in a similar fashion to spatial attention. Specifically, we define

$$\mathbf{v}_{1:T'} = \text{Sigmoid}(\text{ReLU}(\psi \hat{\mathbf{E}}_{1:T'} \mathbf{W}_1^T) \mathbf{W}_2^T) \quad (7)$$

$$\tilde{\mathcal{E}}_{1:T'} = \hat{\mathcal{E}}_{1:T'} \odot \mathbf{V}_{1:T'} \quad (8)$$

where  $\psi^\top = [1/K_E V, \dots, 1/K_E V]$ ,  $\mathbf{W}_1^T \in \mathbb{R}^{T' \times \tau T'}$ ,  $\mathbf{W}_2^T \in \mathbb{R}^{\tau T' \times T'}$  and  $\mathbf{V}_{1:T'} \in \mathbb{R}^{1 \times 1 \times T'}$  is the reshaped temporal attention score vector.

**Graph construction** To build a dynamic graph  $G_{1:T'}$ , we use the spatial-temporally attended brain region embeddings to first construct a dynamic adjacency matrix  $\mathcal{A}_{1:T'}$ . Specifically, at each timepoint we define an adjacency matrix

$$\mathbf{A}_t = \mathbf{E}_t^\top \mathbf{E}_t, \quad \mathbf{E}_t = \text{Softmax}(\tilde{\mathbf{E}}_t) \quad (9)$$

where Softmax( $\cdot$ ) is the softmax activation function applied over the feature dimension, and  $\mathbf{E}_t^\top \mathbf{E}_t$  represents the pairwise inner-product between brain region embeddings. Such a parameterization ensures that each adjacency matrix is weighted  $\mathbf{A}_t \in \mathbb{R}_{\geq 0}^{V \times V}$  and symmetric (or undirected)  $\mathbf{A}_t = \mathbf{A}_t^\top$ . For the dynamic node features  $\mathcal{F}_{1:T'}$ , we instead use the windowed BOLD timeseries  $\tilde{\mathcal{X}}_{1:T'}$  and calculate a correlation coefficient matrix between brain regions  $\tilde{\mathbf{X}}_{i,t}, \tilde{\mathbf{X}}_{j,t} \in \mathbb{R}^P$  such that

$$\mathcal{F}_{i,j,t} = \text{Cov}(\tilde{\mathbf{X}}_{i,t}, \tilde{\mathbf{X}}_{j,t}) / \sigma_{\tilde{\mathbf{X}}_{i,t}} \sigma_{\tilde{\mathbf{X}}_{j,t}} \quad (10)$$

where Cov( $\cdot$ ) denotes cross-covariance and  $\sigma_{\tilde{\mathbf{X}}_{i,t}}$  is the standard deviation of  $i$ -th brain region window at timepoint  $t$ . In other words, we use sliding window correlation matrices as dynamic node features  $\mathbf{F}_t \in [-1, 1]^{V \times V}$  with  $B = V$ .

**Sparsification** By construction, the dynamic adjacency matrix  $\mathcal{A}_{1:T'}$  is a fully connected graph at every timepoint. Not only does this make the adjacency matrices difficult to interpret but it also makes the application of GNNs computationally expensive. To tackle this issue, we propose a version of the soft threshold operator (Donoho 1995) denoted  $f_{\theta_P}(\cdot)$  with learnable parameter  $\theta_P$  to enforce sparsity. Formally,  $f_{\theta_P}(\cdot)$  is applied to each element of  $\mathcal{A}_{1:T'}$  and is defined as

$$f_{\theta_P}(A_{i,j,t}) = \text{ReLU}(A_{i,j,t} - \text{Sigmoid}(\theta_P)) \quad (11)$$

where  $\text{Sigmoid}(\theta_P) = \beta \in [0, 1]$  specifies an edge weight threshold which is learnt during training.

### Dynamic graph classifier

The dynamic graph classifier  $F_{\theta_C}(\cdot)$  next learns a representation of the dynamic brain graph  $F_{\theta_C}(G_{1:T'}) = \mathbf{h}_C$  for use in predicting a class label  $\hat{y}$ . The classifier is a hybrid architecture inspired by the temporal graph convolutional network (Zhao et al. 2019).

**Spatial-temporal feature extraction** We define a block of  $F_{\theta_C}(\cdot)$  as consisting of a GRU layer followed by graph convolution network (GCN) (Kipf and Welling 2016). The GRU first learns temporal features independently for each brain region and then the GCN exploits the topological properties of the learnt dynamic graph by extracting spatial features independently over each timepoint. More formally, let  $\mathbf{F}_{i,1:T'} \in \mathbb{R}^{B \times T'}$  denote the feature timeseries for the  $i$ -th node and suppose  $F_{\theta_C}(\cdot)$  consists of  $L_C$  blocks, then for the  $l$ -th block we have

$$\tilde{\mathbf{H}}_{i,1:T'}^{(l)} = \text{GRU}_\nu(\mathbf{H}_{i,1:T'}^{(l)}) \quad (12)$$

$$\mathbf{H}_t^{(l+1)} = \Omega^{(l)} \tilde{\mathbf{H}}_t^{(l)} \hat{\mathbf{D}}_t^{-1/2} \hat{\mathbf{A}}_t \hat{\mathbf{D}}_t^{-1/2} \quad (13)$$

where  $\mathbf{H}_{i,1:T'}^{(l)} = \mathbf{F}_{i,1:T'}$  are input node features,  $\nu$  and  $\Omega^{(l)} \in \mathbb{R}^{K_C \times K_C}$  are trainable weights,  $\hat{\mathbf{A}}_t = \mathbf{A}_t + \mathbf{I}_V$  is the adjacency matrix with added identity matrix, and  $\hat{\mathbf{D}}_t$  is the degree matrix of  $\hat{\mathbf{A}}_t$ . The final graph-level representation  $\mathbf{h}_C \in \mathbb{R}^{L_C K_C}$  is obtained by concatenating each layers node feature representations along the feature dimension and then summing over nodes and timepoints.

## Loss function

We train DBGSL by minimizing the cross-entropy loss  $L_{CE}(\cdot, \cdot)$  between the actual and predicted label  $y$  and  $\hat{y}$ . Since connected nodes in graphs are more likely to share similar features (McPherson, Smith-Lovin, and Cook 2001), we also add a regularization term to the loss to encourage feature smoothness

$$\mathcal{L}_{FS} = \sum_{t=1}^{T'} \text{Tr}(\mathbf{F}_t^\top \hat{\mathbf{L}}_t \mathbf{F}_t) \quad (14)$$

where  $\text{Tr}(\cdot)$  denotes matrix trace operator, and  $\hat{\mathbf{L}}_t = \mathbf{D}_t^{-1/2} \mathbf{L}_t \mathbf{D}_t^{-1/2}$  is the normalized Laplacian matrix  $\mathbf{L}_t = \mathbf{D}_t - \mathbf{A}_t$  making feature smoothness node degree independent (Ando and Zhang 2006). In addition, to discourage volatile changes in learnt adjacency matrices between time-points we also add a temporal smoothness regularization term

$$\mathcal{L}_{TS} = \sum_{t=1}^{T'-1} \sum_{i=1}^V \sum_{j \leq i} |A_{i,j,t} - A_{i,j,t+1}|. \quad (15)$$

To encourage the learning of a large sparsity parameter  $\theta_P$ , we further add a sparsity regularization term defined

$$\mathcal{L}_{SP} = \sum_{t=1}^{T'} \sum_{i=1}^V \sum_{j \leq i} |A_{i,j,t}|. \quad (16)$$

The final loss function we seek to minimize is  $\mathcal{L} = L_{CE} + \lambda_{FS} \mathcal{L}_{FS} + \lambda_{TS} \mathcal{L}_{TS} + \lambda_{SP} \mathcal{L}_{SP}$  where  $\lambda_{FS}, \lambda_{TS}, \lambda_{SP} \geq 0$  are hyperparameters representing the weighted contribution of each regularization term.

## Experiments

### Gender classification

We evaluate the performance of DBGSL on the task of gender classification, a widely used benchmark for GNN-based models on fMRI data (Kim, Ye, and Kim 2021; Gadgil et al. 2020; Azevedo et al. 2022) since gender differences in the brain are supported by a large body of neuroscience literature (Bell et al. 2006; Mao et al. 2017).

**Datasets** We construct two datasets using publicly available fMRI data from the Human Connectome Project (HCP) S1200 release (Van Essen et al. 2013). For the first dataset, we take resting-state fMRI data (HCP-Rest) from  $N = 1095$  subjects from the first scan-session using left-right phase encoding. Each subject has  $T = 1200$  timepoints with female subjects ( $y = 0$ ) accounting for 54.4% of the dataset with  $C = 2$ . For the second dataset, we use task fMRI data (HCP-Task) from  $N = 926$  subjects performing the emotional task also from the first scan session using left-right phase encoding. Each subject has  $T = 246$  timepoints with female subjects ( $y = 0$ ) accounting for 51.2% of the dataset. The fMRI data is parcellated into  $V = 243$  brain region BOLD timeseries (210 cortical, 36 subcortical) using the Brainnetome atlas (Fan et al. 2016). Finally, all timeseries are transformed into z-scores to remove amplitude effects.

**Baselines** We compare DBGSL against a range of baseline models, all with publicly available code. The baselines are broadly grouped by whether they take as input static FC, dynamic FC, or region-wise BOLD timeseries. For static FC baselines, we compare against kernel ridge regression (KRR) from He et al. (2020) and the support vector machine (SVM) from Abraham et al. (2017), both utilizing linear kernels and taking as input vectorized static FCMs. In addition, for deep learning baselines we include the multilayer perceptron (MLP) and BrainnetCNN (BNCNN) from Kawahara et al. (2017) where the latter uses specially designed convolutional filters for extracting topological features from static FCMs. For a GSL baseline, we implement FBNetGen (FBNETGEN) from Kan et al. (2022) which learns static brain graph representations from BOLD timeseries using an LSTM and GNN. On the other hand, for dynamic FC we compare against two GNN baselines ST-GCN (STGCN) proposed by Gadgil et al. (2020) and STAGIN from Kim, Ye, and Kim (2021) which learns dynamic graph representations using spatial-temporal attention within a transformer framework. Finally, we follow the LSTM implement of Hebling Vieira et al. (2021) to compare against a baseline which learns directly from BOLD timeseries.

**Implementation** All models are implemented using PyTorch (Paszke et al. 2019) on a Linux server (Debian 5.10.113-1) with a NVIDIA RTX A6000 GPU with 48 GB memory. Both datasets are split into 80%/10%/10% training/validation/test datasets maintaining class proportions as well as ensuring subjects from the same family were not were split across dataset splits. For fairness of comparison, all models are trained using the Adam optimizer (Kingma and Ba 2014) with decoupled weight decay regularization (Loshchilov and Hutter 2017). We use the hyperparameter settings described in the original implementation of each baseline model. For DBGSL, we tune all hyperparameters on the validation dataset. Specifically, for the dynamic graph learner  $F_{\theta_G}(\cdot)$  the optimal values for window length and stride are  $P = 50, S = 3$  and  $P = 30, S = 1$  for HCP-Rest and HCP-Task respectively, number of layers  $L_G = 4$ , number of features  $K_G = 64$ , filter sizes  $S_1, S_2, S_3 = 4, 8, 16$ , embedding size  $K_E = 16$ , bottleneck  $\tau = 1/2$ , and initial sparsity  $\theta_s = -5$ . For the graph classifier  $F_{\theta_C}(\cdot)$  the optimal values for number of layers  $L_C = 3$  and number of features  $K_C = 64$ . For the regularization terms  $\lambda_{FS} = 1e-4, \lambda_{TS} = 1e-4$ , and  $\lambda_{SP} = 1e-3$ . On both datasets, we use a learning rate of  $1e-3$ , weight decay  $1e-4$ , and train for 1000 epochs with a batch size of 15. To avoid computational overload and add stochastic augmentation, the time dimension of training samples is randomly sampled to be  $T = 600$  for HCP-Rest and  $T = 150$  for HCP-Task following Kim, Ye, and Kim (2021). To prevent overfitting, early-stopping was used with a patience of 15 based on the lowest accuracy on the validation dataset. Finally, all models were trained 5 times using a different random seed as well as dataset splits.

**Metrics** We evaluate final model performance across all test dataset splits using mean accuracy and area under the receiver operator curve (AUROC) since classes are balanced. In order to compare models we use the almost stochastic or-

Model	FC	HCP-Rest		HCP-Task	
		Accuracy (% , $\uparrow$ )	AUROC ( $\uparrow$ )	Accuracy (% , $\uparrow$ )	AUROC ( $\uparrow$ )
KRC	S	83.16 $\pm$ 2.14 *	0.9170 $\pm$ 0.0230 *	80.37 $\pm$ 2.42 *	0.8964 $\pm$ 0.0209 *
SVM	S	81.50 $\pm$ 2.17 *	0.9027 $\pm$ 0.0480 *	81.63 $\pm$ 2.01 *	0.9077 $\pm$ 0.0231 *
MLP	S	81.47 $\pm$ 3.67 *	0.9091 $\pm$ 0.0315 *	81.10 $\pm$ 3.85 *	0.8837 $\pm$ 0.0280 *
LSTM	-	81.50 $\pm$ 1.41 *	0.9058 $\pm$ 0.0910 *	77.24 $\pm$ 4.53 *	0.8526 $\pm$ 0.0210 *
BNCNN	S	76.83 $\pm$ 8.34 *	0.6156 $\pm$ 0.0936 *	70.66 $\pm$ 9.20 *	0.5945 $\pm$ 0.0558 *
STGCN	D	62.63 $\pm$ 5.03 *	0.6991 $\pm$ 0.0296 *	54.87 $\pm$ 3.77 *	0.5629 $\pm$ 0.0797 *
FBNETGEN	S	81.57 $\pm$ 3.25 *	0.8967 $\pm$ 0.0190 *	77.16 $\pm$ 4.36 *	0.8548 $\pm$ 0.0358 *
STAGIN	D	83.13 $\pm$ 2.82 *	0.9063 $\pm$ 0.0480 *	81.16 $\pm$ 2.14 *	0.9028 $\pm$ 0.0130 *
DBGSL	D	<b>88.32 <math>\pm</math> 2.48</b>	<b>0.9543 <math>\pm</math> 0.0224</b>	<b>89.54 <math>\pm</math> 2.89</b>	<b>0.9416 <math>\pm</math> 0.0224</b>

Table 1: Gender classification results on HCP-Rest and HCP-Task. Results are mean plus/minus standard deviation across 5 test dataset splits. First and second-best results are shown in **bold** and underlined respectively. Statistically significant results marked with \*. Models grouped by type of functional connectivity (FC) (S = static, D = dynamic, - = BOLD timeseries).

der (ASO) (Del Barrio, Cuesta-Albertos, and Matrán 2018; Dror, Shlomov, and Reichart 2019) test of statistical significance implemented by Ulmer, Hardmeier, and Frelsen (2022). For all tests, the significance level is set to  $\alpha = 0.05$  and adjusted using the Bonferroni correction (Bonferroni 1936) when making multiple comparisons.

**Results** Classification results are summarized in Table 1. Clearly DBGSL is the best performing model on both datasets as measured by accuracy and AUROC. Specifically, on HCP-Rest DBGSL outperforms the second-best baseline KRC in terms of accuracy by 5.16 percentage points (pp) whereas on HCP-Task the second-best baseline SVM is outperformed by DBGSL by 8.38 pp, with both gains being statistically significant. Interestingly, the two linear baselines KRC and SVM when compared to the deep learning baselines MLP, LSTM, BNCNN, STGCN, FBNETGEN, and STAGIN either outperform or the difference in metrics is not statistically significant, a finding similar to He et al. (2020). We attribute the superior performance of DBGSL to the dependency structure being learnt rather than fixed (DBGSL 89.54% vs STAGIN 81.16% HCP-Task), and when learnt, being dynamic rather than static (DBGSL 88.32% vs FBNETGEN 81.57% HCP-Rest).

### Ablation study

We conduct an ablation study to investigate the impact on performance of DBGSL without (w/o) key model components. Specifically, within the dynamic graph learner  $F_{\theta_G}(\cdot)$  we replace the I-TCN embedding network  $f_{\theta_E}(\cdot)$  with a 1D convolution with kernel size 4 (w/o inception), remove spatial attention  $f_{\theta_S}(\cdot)$  (w/o spatial att.), remove temporal attention  $f_{\theta_T}(\cdot)$  (w/o temporal att.), and remove the sparsity layer  $f_{\theta_P}(\cdot)$  with  $\lambda_{SP} = 0$  (w/o sparsity). In addition, we also remove feature smoothness  $\lambda_{FS} = 0$  (w/o feature reg.) and temporal smoothness  $\lambda_{TS} = 0$  (w/o temporal reg.) regularization terms.

**Results** Table 2 summarizes the results of the ablation study. Clearly, the introduction of spatial attention significantly improves accuracy across both datasets ( $\uparrow$  2.27 pp

Model	Accuracy (% , $\uparrow$ )	
	HCP-Rest	HCP-Task
DBGSL	<b>88.32 <math>\pm</math> 2.48</b>	<b>89.54 <math>\pm</math> 2.89</b>
- w/o inception	87.20 $\pm$ 2.69 *	88.83 $\pm$ 2.94
- w/o spatial att.	86.05 $\pm$ 3.06 *	87.01 $\pm$ 3.80 *
- w/o temporal att.	88.06 $\pm$ 2.65	88.86 $\pm$ 2.94
- w/o sparsity	87.31 $\pm$ 2.77 *	87.31 $\pm$ 2.77 *
- w/o feature reg.	88.29 $\pm$ 2.41	88.49 $\pm$ 3.24
- w/o temporal reg.	88.12 $\pm$ 2.21	88.53 $\pm$ 3.25

Table 2: Ablation study results on HCP-Rest and HCP-Task. Results are mean plus/minus standard deviation across 5 test dataset splits. Best results are shown in **bold**. Statistically significant results are marked with \*.

HCP-Rest vs  $\uparrow$  2.53 pp HCP-Rest) since it allows for task-aware spatial relationships between brain regions to be built into the dynamic graph adjacency matrix for use by the graph classifier. Similarly, sparsity also significantly improves accuracy ( $\uparrow$  1.01 pp HCP-Rest vs  $\uparrow$  2.23 pp HCP-Rest) since it removes noisy edges from the adjacency matrix thereby reducing errors from being propagated to node representations. Finally, the effect of inception is significant for HCP-Rest ( $\uparrow$  1.12 pp) but only marginal for HCP-Task ( $\uparrow$  0.71 pp) which might be explained by the fact that the BOLD timeseries from the former dataset are collected over a longer time period than the latter thereby benefiting more from larger kernel sizes being able to extract longer temporal patterns.

### Hyperparameter sensitivity

We conduct a sensitivity analysis on the main hyperparameters which influence the complexity of DBGSL. In particular, for the dynamic graph learner  $F_{\theta_G}(\cdot)$  we vary window length  $P$ , window stride  $S$ , embedding size  $K_E$ , and number of layers  $L_G$ . On the other hand, for the dynamic graph classifier  $F_{\theta_C}(\cdot)$  we vary number of layers  $L_C$  and number of features  $K_C$ . For each experiment, we change the param-

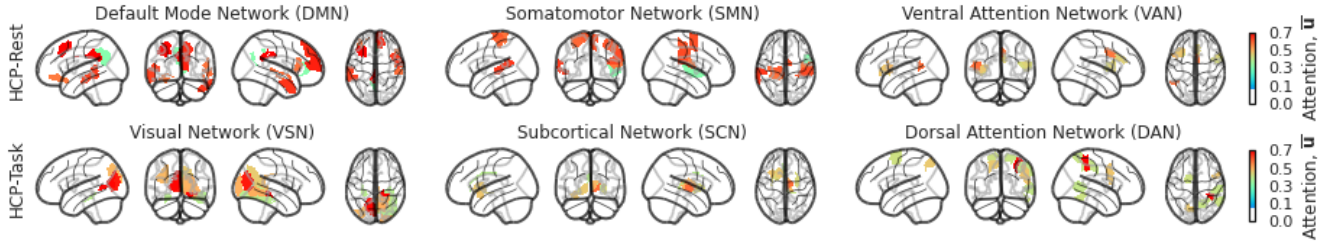


Figure 2: Top 20% of spatially attended brain regions for HCP-Rest and HCP-Task. Regions are grouped by intrinsic connectivity networks from Yeo et al. (2011). Only the top-3 networks with the most number of regions are shown (descending order).

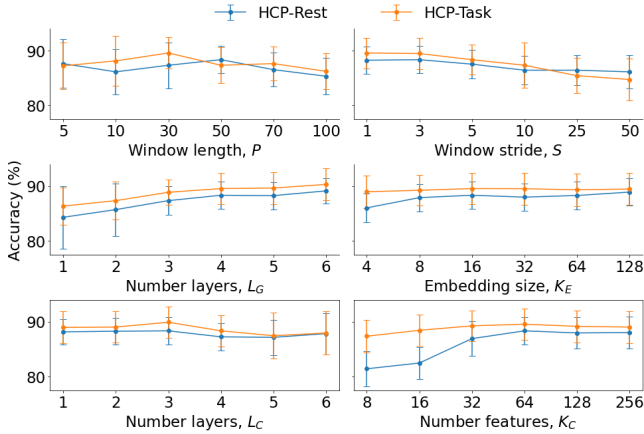


Figure 3: Sensitivity analysis results on HCP-Rest and HCP-Task. Results are mean and standard deviation across 5 test dataset splits

eter under investigation and fix other parameters to their optimally tuned values.

**Results** Figure 3 shows the results of the hyperparameter sensitivity analysis. On both HCP-Rest and HCP-Task we see that increasing window size  $P$  decreases accuracy which we attribute to the fact that more data within a window makes it harder for the dynamic graph learner to identify fast changes between brain regions that are task discriminative. A similar relationship holds for increasing window stride  $P$  due to the loss of information among contiguous regions of BOLD timeseries when building dynamic graphs. Furthermore, increasing the depth of information propagation beyond 3 hops in the dynamic graph classifier decreases performance as shown by the number of layers  $L_C$ . Finally, increasing the number of layers  $L_G$  and embedding size  $K_E$  in the graph learner as well as the number of features  $K_C$  in the graph classifier each show diminishing returns on performance gains.

### Interpretability

To find which brain regions from the learnt dynamic brain graphs are most gender-discriminative, we first average the spatial attention score vectors over time  $\bar{\mathbf{u}} = 1/T' \sum_{t=1}^{T'} \mathbf{u}_t$

and normalize the scores to the range  $[0, 1]$ . We then take all regions falling within the top 20% across all subjects and plot them with respect to the intrinsic connectivity networks of Yeo et al. (2011).

**Results** Figure 2 summarizes the interpretability results. For HCP-Rest, 25.5% of the highest attention scores are within the default mode network (DMN), a key brain circuit that is consistently observed in resting-state fMRI studies (Mak et al. 2017; Satterthwaite et al. 2015). Within the DMN the brain regions with the highest gender-prediction ability are localized in the dorsal anterior cingulate cortex, middle frontal gyrus, and posterior superior temporal cortex. These fronto-temporal brain regions are key components of the theory of mind network, which underlies a meta-cognitive function in which females usually excel (Adenzato et al. 2017). Another key region in theory of mind tasks, the posterior superior temporal cortex is found to reliably predict gender within the ventral attention network (VAN). For HCP-Task, 30.6% of the highest attention scores are found in the parahippocampal gyrus, medial occipital cortex, and superior parietal lobule which form a posterior visual network (VSN). The fact that such regions best discriminate males from females reflects differences in the ability to process emotional content and/or gender-related variability in directing attention to certain features of emotional stimuli (Mackiewicz et al. 2006), like the facial expressions from the HCP task paradigm (Markett et al. 2020).

### Conclusion

In conclusion, we propose Dynamic Brain Graph Structure Learning (DBGSL), an end-to-end trainable model that learns the optimal time-varying dependency structure of fMRI data in the form of a dynamic brain graph. To the best of our knowledge, we are the first to propose and address the dynamic GSL problem via GNN-based deep learning on fMRI timeseries data. Central to our approach is the use of spatial-temporal attention to exploit the inherent inter and intra relationships of brain region timeseries. We demonstrate via extensive experiments on two real-world fMRI datasets that DBGSL achieves state-of-the-art results on the benchmark task of gender classification. Future research directions will be to learn the optimal window size and stride during model training as well as using electroencephalogram (EEG) data to learn dynamic FC alongside fMRI.

## Acknowledgements

This work is supported by The Alan Turing Institute under the EPSRC grant EP/N510129/1. Data were provided [in part] by the Human Connectome Project, WU-Minn Consortium (Principal Investigators: David Van Essen and Kamil Ugurbil; 1U54MH091657) funded by the 16 NIH Institutes and Centers that support the NIH Blueprint for Neuroscience Research; and by the McDonnell Center for Systems Neuroscience at Washington University.

## References

- Abraham, A.; Milham, M. P.; Di Martino, A.; Craddock, R. C.; Samaras, D.; Thirion, B.; and Varoquaux, G. 2017. Deriving reproducible biomarkers from multi-site resting-state data: An Autism-based example. *NeuroImage*, 147: 736–745.
- Adenzato, M.; Brambilla, M.; Manenti, R.; De Lucia, L.; Trojano, L.; Garofalo, S.; Enrici, I.; and Cotelli, M. 2017. Gender differences in cognitive Theory of Mind revealed by transcranial direct current stimulation on medial prefrontal cortex. *Scientific reports*, 7(1): 1–9.
- Ando, R.; and Zhang, T. 2006. Learning on graph with Laplacian regularization. *Advances in neural information processing systems*, 19.
- Azevedo, T.; Campbell, A.; Romero-Garcia, R.; Passamonti, L.; Bethlehem, R. A.; Liò, P.; and Toschi, N. 2022. A deep graph neural network architecture for modelling spatio-temporal dynamics in resting-state functional MRI data. *Medical Image Analysis*, 79: 102471.
- Bell, E. C.; Willson, M. C.; Wilman, A. H.; Dave, S.; and Silverstone, P. H. 2006. Males and females differ in brain activation during cognitive tasks. *Neuroimage*, 30(2): 529–538.
- Bonferroni, C. 1936. Teoria statistica delle classi e calcolo delle probabilita. *Pubblicazioni del R Istituto Superiore di Scienze Economiche e Commerciali di Firenze*, 8: 3–62.
- Calhoun, V. D.; Miller, R.; Pearlson, G.; and Adali, T. 2014. The chronnectome: time-varying connectivity networks as the next frontier in fMRI data discovery. *Neuron*, 84(2): 262–274.
- Cao, D.; Wang, Y.; Duan, J.; Zhang, C.; Zhu, X.; Huang, C.; Tong, Y.; Xu, B.; Bai, J.; Tong, J.; et al. 2020. Spectral temporal graph neural network for multivariate time-series forecasting. *Advances in neural information processing systems*, 33: 17766–17778.
- Chang, C.; and Glover, G. H. 2010. Time–frequency dynamics of resting-state brain connectivity measured with fMRI. *Neuroimage*, 50(1): 81–98.
- Cho, K.; Van Merriënboer, B.; Bahdanau, D.; and Bengio, Y. 2014. On the properties of neural machine translation: Encoder-decoder approaches. *arXiv preprint arXiv:1409.1259*.
- Del Barrio, E.; Cuesta-Albertos, J. A.; and Matrán, C. 2018. An optimal transportation approach for assessing almost stochastic order. In *The Mathematics of the Uncertain*, 33–44. Springer.
- Donoho, D. L. 1995. De-noising by soft-thresholding. *IEEE transactions on information theory*, 41(3): 613–627.
- Dror, R.; Shlomov, S.; and Reichart, R. 2019. Deep Dominance - How to Properly Compare Deep Neural Models. In Korhonen, A.; Traum, D. R.; and Márquez, L., eds., *Proceedings of the 57th Conference of the Association for Computational Linguistics, ACL 2019, Florence, Italy, July 28- August 2, 2019, Volume 1: Long Papers*, 2773–2785. Association for Computational Linguistics.
- Fan, L.; Li, H.; Zhuo, J.; Zhang, Y.; Wang, J.; Chen, L.; Yang, Z.; Chu, C.; Xie, S.; Laird, A. R.; et al. 2016. The human brainnetome atlas: a new brain atlas based on connectional architecture. *Cerebral cortex*, 26(8): 3508–3526.
- Fan, L.; Su, J.; Qin, J.; Hu, D.; and Shen, H. 2020. A deep network model on dynamic functional connectivity with applications to gender classification and intelligence prediction. *Frontiers in neuroscience*, 14: 881.
- Franceschi, L.; Niepert, M.; Pontil, M.; and He, X. 2019. Learning discrete structures for graph neural networks. In *International conference on machine learning, 1972–1982*. PMLR.
- Friston, K. J. 1994. Functional and effective connectivity in neuroimaging: a synthesis. *Human brain mapping*, 2(1-2): 56–78.
- Gadgil, S.; Zhao, Q.; Pfefferbaum, A.; Sullivan, E. V.; Adeli, E.; and Pohl, K. M. 2020. Spatio-temporal graph convolution for resting-state fmri analysis. In *International Conference on Medical Image Computing and Computer-Assisted Intervention*, 528–538. Springer.
- Gao, Y.; and No, A. 2022. Age Estimation from fMRI Data Using Recurrent Neural Network. *Applied Sciences*, 12(2): 749.
- Hahnloser, R. H.; Sarpeshkar, R.; Mahowald, M. A.; Douglas, R. J.; and Seung, H. S. 2000. Digital selection and analogue amplification coexist in a cortex-inspired silicon circuit. *nature*, 405(6789): 947–951.
- He, T.; Kong, R.; Holmes, A. J.; Nguyen, M.; Sabuncu, M. R.; Eickhoff, S. B.; Bzdok, D.; Feng, J.; and Yeo, B. T. 2020. Deep neural networks and kernel regression achieve comparable accuracies for functional connectivity prediction of behavior and demographics. *NeuroImage*, 206: 116276.
- Hebling Vieira, B.; Dubois, J.; Calhoun, V. D.; and Garrido Salmon, C. E. 2021. A deep learning based approach identifies regions more relevant than resting-state networks to the prediction of general intelligence from resting-state fMRI. *Human Brain Mapping*, 42(18): 5873–5887.
- Hochreiter, S.; and Schmidhuber, J. 1997. Long short-term memory. *Neural computation*, 9(8): 1735–1780.
- Hu, J.; Shen, L.; and Sun, G. 2018. Squeeze-and-excitation networks. In *Proceedings of the IEEE conference on computer vision and pattern recognition*, 7132–7141.
- Huang, S.-G.; Xia, J.; Xu, L.; and Qiu, A. 2022. Spatio-temporal directed acyclic graph learning with attention mechanisms on brain functional time series and connectivity. *Medical Image Analysis*, 77: 102370.
- Ioffe, S.; and Szegedy, C. 2015. Batch normalization: Accelerating deep network training by reducing internal covariate shift. In *International conference on machine learning*, 448–456. PMLR.
- Jie, B.; Liu, M.; Lian, C.; Shi, F.; and Shen, D. 2020. Designing weighted correlation kernels in convolutional neural networks for functional connectivity based brain disease diagnosis. *Medical image analysis*, 63: 101709.
- Kan, X.; Cui, H.; Lukemire, J.; Guo, Y.; and Yang, C. 2022. Fbnetgen: Task-aware gnn-based fmri analysis via functional brain network generation. *arXiv preprint arXiv:2205.12465*.
- Kawahara, J.; Brown, C. J.; Miller, S. P.; Booth, B. G.; Chau, V.; Grunau, R. E.; Zwicker, J. G.; and Hamarneh, G. 2017. BrainNetCNN: Convolutional neural networks for brain networks; towards predicting neurodevelopment. *NeuroImage*, 146: 1038–1049.
- Kim, B.-H.; and Ye, J. C. 2020. Understanding graph isomorphism network for rs-fMRI functional connectivity analysis. *Frontiers in neuroscience*, 630.
- Kim, B.-H.; Ye, J. C.; and Kim, J.-J. 2021. Learning dynamic graph representation of brain connectome with spatio-temporal attention. *Advances in Neural Information Processing Systems*, 34: 4314–4327.



- Kingma, D. P.; and Ba, J. 2014. Adam: A method for stochastic optimization. *arXiv preprint arXiv:1412.6980*.
- Kipf, T. N.; and Welling, M. 2016. Semi-supervised classification with graph convolutional networks. *arXiv preprint arXiv:1609.02907*.
- Korhonen, O.; Zanin, M.; and Papo, D. 2021. Principles and open questions in functional brain network reconstruction. *Human Brain Mapping*, 42(11): 3680–3711.
- Li, X.; Zhou, Y.; Dvornik, N.; Zhang, M.; Gao, S.; Zhuang, J.; Scheinost, D.; Staib, L. H.; Ventola, P.; and Duncan, J. S. 2021. BrainGnn: Interpretable brain graph neural network for fmri analysis. *Medical Image Analysis*, 74: 102233.
- Loshchilov, I.; and Hutter, F. 2017. Decoupled weight decay regularization. *arXiv preprint arXiv:1711.05101*.
- Mackiewicz, K. L.; Sarinopoulos, I.; Cleven, K. L.; and Nitschke, J. B. 2006. The effect of anticipation and the specificity of sex differences for amygdala and hippocampus function in emotional memory. *Proceedings of the National Academy of Sciences*, 103(38): 14200–14205.
- Mahmood, U.; Fu, Z.; Calhoun, V. D.; and Plis, S. 2021. A deep learning model for data-driven discovery of functional connectivity. *Algorithms*, 14(3): 75.
- Mak, L. E.; Minuzzi, L.; MacQueen, G.; Hall, G.; Kennedy, S. H.; and Milev, R. 2017. The default mode network in healthy individuals: a systematic review and meta-analysis. *Brain connectivity*, 7(1): 25–33.
- Mao, N.; Zheng, H.; Long, Z.; Yao, L.; and Wu, X. 2017. Gender differences in dynamic functional connectivity based on resting-state fMRI. In *2017 39th Annual International Conference of the IEEE Engineering in Medicine and Biology Society (EMBC)*, 2940–2943. IEEE.
- Markett, S.; Jawinski, P.; Kirsch, P.; and Gerchen, M. F. 2020. Specific and segregated changes to the functional connectome evoked by the processing of emotional faces: A task-based connectome study. *Scientific Reports*, 10(1): 1–14.
- McPherson, M.; Smith-Lovin, L.; and Cook, J. M. 2001. Birds of a feather: Homophily in social networks. *Annual review of sociology*, 415–444.
- Mohanty, R.; Sethares, W. A.; Nair, V. A.; and Prabhakaran, V. 2020. Rethinking measures of functional connectivity via feature extraction. *Scientific reports*, 10(1): 1–17.
- Oord, A. v. d.; Dieleman, S.; Zen, H.; Simonyan, K.; Vinyals, O.; Graves, A.; Kalchbrenner, N.; Senior, A.; and Kavukcuoglu, K. 2016. Wavenet: A generative model for raw audio. *arXiv preprint arXiv:1609.03499*.
- Paszke, A.; Gross, S.; Massa, F.; Lerer, A.; Bradbury, J.; Chanan, G.; Killeen, T.; Lin, Z.; Gimelshein, N.; Antiga, L.; et al. 2019. Pytorch: An imperative style, high-performance deep learning library. *arXiv preprint arXiv:1912.01703*.
- Riaz, A.; Asad, M.; Alonso, E.; and Slabaugh, G. 2020. DeepFMRI: End-to-end deep learning for functional connectivity and classification of ADHD using fMRI. *Journal of neuroscience methods*, 335: 108506.
- Satterthwaite, T. D.; Wolf, D. H.; Roalf, D. R.; Ruparel, K.; Erus, G.; Vandekar, S.; Gennatas, E. D.; Elliott, M. A.; Smith, A.; Hakonarson, H.; et al. 2015. Linked sex differences in cognition and functional connectivity in youth. *Cerebral cortex*, 25(9): 2383–2394.
- Shang, C.; Chen, J.; and Bi, J. 2021. Discrete Graph Structure Learning for Forecasting Multiple Time Series. *arXiv preprint arXiv:2101.06861*.
- Sporns, O. 2022. Graph theory methods: applications in brain networks. *Dialogues in clinical neuroscience*.
- Szegedy, C.; Liu, W.; Jia, Y.; Sermanet, P.; Reed, S.; Anguelov, D.; Erhan, D.; Vanhoucke, V.; and Rabinovich, A. 2015. Going deeper with convolutions. In *Proceedings of the IEEE conference on computer vision and pattern recognition*, 1–9.
- Ulmer, D.; Hardmeier, C.; and Frellsen, J. 2022. deep-significance-Easy and Meaningful Statistical Significance Testing in the Age of Neural Networks. *arXiv preprint arXiv:2204.06815*.
- Van Essen, D. C.; Smith, S. M.; Barch, D. M.; Behrens, T. E.; Yacoub, E.; Ugurbil, K.; Consortium, W.-M. H.; et al. 2013. The WU-Minn human connectome project: an overview. *Neuroimage*, 80: 62–79.
- Wang, H. E.; Bénar, C. G.; Quilichini, P. P.; Friston, K. J.; Jirsa, V. K.; and Bernard, C. 2014. A systematic framework for functional connectivity measures. *Frontiers in neuroscience*, 8: 405.
- Wang, J.; Zuo, X.; and He, Y. 2010. Graph-based network analysis of resting-state functional MRI. *Frontiers in systems neuroscience*, 16.
- Wang, Y.; Kang, J.; Kemmer, P. B.; and Guo, Y. 2016. An efficient and reliable statistical method for estimating functional connectivity in large scale brain networks using partial correlation. *Frontiers in neuroscience*, 10: 123.
- Wu, Z.; Pan, S.; Chen, F.; Long, G.; Zhang, C.; and Philip, S. Y. 2020a. A comprehensive survey on graph neural networks. *IEEE transactions on neural networks and learning systems*, 32(1): 4–24.
- Wu, Z.; Pan, S.; Long, G.; Jiang, J.; Chang, X.; and Zhang, C. 2020b. Connecting the dots: Multivariate time series forecasting with graph neural networks. In *Proceedings of the 26th ACM SIGKDD International Conference on Knowledge Discovery & Data Mining*, 753–763.
- Wu, Z.; Pan, S.; Long, G.; Jiang, J.; and Zhang, C. 2019. Graph wavenet for deep spatial-temporal graph modeling. *arXiv preprint arXiv:1906.00121*.
- Yan, B.; Xu, X.; Liu, M.; Zheng, K.; Liu, J.; Li, J.; Wei, L.; Zhang, B.; Lu, H.; and Li, B. 2020. Quantitative identification of major depression based on resting-state dynamic functional connectivity: A machine learning approach. *Frontiers in neuroscience*, 14: 191.
- Yeo, B. T.; Krienen, F. M.; Sepulcre, J.; Sabuncu, M. R.; Lashkari, D.; Hollinshead, M.; Roffman, J. L.; Smoller, J. W.; Zöllei, L.; Polimeni, J. R.; et al. 2011. The organization of the human cerebral cortex estimated by intrinsic functional connectivity. *Journal of neurophysiology*.
- Zalesky, A.; and Breakspear, M. 2015. Towards a statistical test for functional connectivity dynamics. *Neuroimage*, 114: 466–470.
- Zhang, Y.; and Huang, H. 2019. New graph-blind convolutional network for brain connectome data analysis. In *International Conference on Information Processing in Medical Imaging*, 669–681. Springer.
- Zhang, Y.; Tetrel, L.; Thirion, B.; and Bellec, P. 2021. Functional annotation of human cognitive states using deep graph convolution. *NeuroImage*, 231: 117847.
- Zhao, K.; Duka, B.; Xie, H.; Oathes, D. J.; Calhoun, V.; and Zhang, Y. 2022. A dynamic graph convolutional neural network framework reveals new insights into connectome dysfunctions in ADHD. *Neuroimage*, 246: 118774.
- Zhao, L.; Song, Y.; Zhang, C.; Liu, Y.; Wang, P.; Lin, T.; Deng, M.; and Li, H. 2019. T-gcn: A temporal graph convolutional network for traffic prediction. *IEEE Transactions on Intelligent Transportation Systems*, 21(9): 3848–3858.

Zhu, Y.; Xu, W.; Zhang, J.; Du, Y.; Zhang, J.; Liu, Q.; Yang, C.; and Wu, S. 2021. A Survey on Graph Structure Learning: Progress and Opportunities. *arXiv e-prints*, arXiv-2103.